THE JOURNAL OF NAVIGATION (2020), **73**, 530–546.
doi:10.1017/S037346331900078X

Refinement of GLONASS Phase Inter-Frequency Biases and Their Applications on Single-Epoch Ambiguity Fixing

Yumiao Tian[1,2]

[1](*Faculty of Geosciences and Environmental Engineering, Southwest Jiaotong University, Chengdu, Sichuan 611756, China*)
[2](*State-Province Joint Engineering Laboratory of Spatial Information Technology for High-Speed Railway Safety, Chengdu, Sichuan 611756, China*)
(E-mail: tymr@163.com)

Carrier-phase inter-frequency bias (IFB) exists in GLObal NAvigation Satellite System (GLONASS) baselines when receivers of different brands are used. Those biases need to be calibrated in GLONASS data processing to derive precise fixed solutions. Consequently, the accuracy of the IFB calibration affects ambiguity fixing, and low-accuracy IFB values in the calibration will degrade the positioning results. Hitherto, at least two IFB rate value sets for various receiver brands have been given in previous studies. Some of the differences between the value sets exceed 2 mm/FN (frequency number) and the effects of those differences on ambiguity fixing have not been investigated until now. This study showed that ambiguity fixing in GLONASS single-epoch positioning is very sensitive to the accuracy of the IFB rates. Even errors of millimetres can seriously lower the empirical success rate. The short baselines from the Global Navigation Satellite System (GNSS, which includes Russian GLONASS) networks of the International GNSS Service and the Regional Reference Frame Sub-Commission for Europe were employed to obtain more accurate IFB rate estimates with the proposed two-dimensional particle filtering. Afterwards, the IFB estimates were statistically refined by the least-squares method. Experiments showed that when the refined IFB rates were used in the IFB calibration, the empirical success rates of ambiguity fixing in GLONASS single-epoch positioning were largely improved compared with the values given before, improvements such as 20·6% for a Septentrio and Leica receiver combination.

KEYWORDS

1. GLONASS. 2. Phase IFB Rate. 3. Ambiguity Fixing. 4. Single-Epoch Positioning.

Submitted: 5 January 2019. Accepted: 17 August 2019. First published online: 8 November 2019.

1. INTRODUCTION. GLObal NAvigation Satellite System (GLONASS) signals are based on a frequency division multiple access (FDMA) technique leading to different signal satellite frequencies. Although the recently launched GLONASS satellites also emit CDMA signals from the systems of GPS/Galileo/BDS, FDMA signals cannot be replaced

within a short time frame and so will continue to be used in the coming decades. The variable-frequency FDMA signals pass through different hardware in Global Navigation Satellite System (GNSS, which includes Russian GLONASS) receivers (Pratt et al., 1998; Zinoviev et al., 2009; Sleewagen et al., 2012) and thus the delays caused by the hardware may be different when receivers from different manufacturers are employed in relative positioning, leading to non-zero phase inter-frequency biases (IFB), which degrade the integer ambiguity fixing.

The phase IFBs of FDMA signals are linear with the frequency number ranging from −7 to 6. As the values of the IFB rate for a series of GLONASS receivers are very stable, employing the linear correction model with a known linear rate can successfully remove the carrier-phase IFBs in the GLONASS baseline resolution (Wanninger, 2012; Al-Shaery, 2013; Tian et al., 2015). Banville et al. (2013) proposed a method to eliminate the IFB parameter by sacrificing one double-difference (DD) equation. This method assumes that the IFB is generated by the misalignment of the code and the phase measurements (Sleewagen et al., 2012; Banville et al., 2013). Although the equations differ from the former method, the IFB-related unknown items in this method are also approximately linear because the wavelength differences between all adjacent frequencies are very similar (the residuals are around 10^{-7} m when fitting GLONASS frequency band L1 wavelengths against frequency numbers with a linear model). Therefore, the two approaches are mathematically similar. However, if the accurate a priori IFB rates are available, calibrating IFB by the linear model in advance is still preferable.

To serve the applications of the GNSS community, at least two value sets of carrier-phase IFB rates have been calculated and revealed to date, including the values given in research undertaken by Wanninger (2012) and Jiang et al., (2017). The differences between the two value sets can exceed 2 mm/FN, for example, 2·8 mm/FN for the Trimble and Ashtech receiver combination. This difference is amplified by the coefficients of the linear model in the IFB rate calibration. The coefficient is the difference of the satellite frequency numbers in the DD phase equation and can be as large as 13. Thus, in the worst case, a 2·8 mm/FN difference on the IFB rate could cause an error of 3·64 cm in the phase model.

The difference between the two value sets of IFB rates may have resulted from the long baselines employed in the previous studies (Wanninger, 2012; Jiang et al., 2017). Using long baselines can increase the number of available GNSS stations and therefore include more receiver types in the investigation. However, the disadvantages of using long baselines are also obvious: errors from sources such as the ionosphere, troposphere, even ocean tides can be large, which potentially decrease the accuracy of the IFB rate estimates. Therefore, short baselines that are almost free of such errors are more appropriate for IFB value estimations. In this study, short baselines in the International GNSS Service (IGS) and Regional Reference Frame Sub-Commission for Europe (EUREF) GNSS networks were employed to estimate the IFB rate values; the least-squares method was then used to statistically refine the results.

The application of IFB rates on GLONASS single-epoch ambiguity fixing was subsequently investigated. Single-epoch precise positioning employs both the phase and pseudorange observations of one epoch to resolve the baseline. The instantaneous solution is provided independently from epoch to epoch without initialisation or reinitialisation. Consequently, this method can process the data rapidly and is immune to cycle slips on the carrier phase (Parkins, 2011; Paziewski and Wielgosz, 2014). Due to the improvement of the satellite ephemeris and the increase in available GNSS satellites, the advantage

https://doi.org/10.1017/S037346331900078X Published online by Cambridge University Press

of the single-epoch positioning has been enhanced and is becoming increasingly useful, especially in challenging environments.

The content of this manuscript is organised as follows. The IFB rate estimation approach is presented in Section 2. Section 3 introduces the data used in the study. Section 4 presents the results of the estimates and the refined IFB rate values. The application of the refined IFB rate values on single-epoch GLONASS ambiguity fixing is investigated in Section 5, and the conclusions are given in Section 6.

2. IFB DETERMINATION METHOD OF THE TWO-DIMENSIONAL PARTICLE FILTERING APPROACH.

The particle filtering approach has been proposed to estimate IFB rates (Tian et al., 2015, 2018a). This method is able to estimate IFB rates from long-term observations or in real-time and can work for both short- and long baselines (Liu et al., 2016). In this research, only baselinesshorter than 15 km were employed to guarantee high accuracy. In this case, the receiver clock and satellite clock are cancelled. The tropospheric and ionospheric delays are largely reduced, and the multipath effects are neglected. The observation model (Model 1) can be expressed as Equation (1).

$$P_{ab}^{ij} = \rho_{ab}^{ij} + d_{ab}^{ij} + \varepsilon_{ab}^{ij}, \tag{1a}$$

$$\lambda^j \Phi_{ab}^j - \lambda^i \Phi_{ab}^i = \rho_{ab}^{ij} + \lambda^j N_{ab}^j - \lambda^i N_{ab}^i + \left(k^j - k^i\right) \Delta\gamma_{ab} + \xi_{ab}^{ij}, \tag{1b}$$

where P is the code pseudorange measurement; ij and ab refer to the satellites and the observation stations in the DD models, respectively; ρ is the initial value of the distance; d_{ab}^{ij} is the between receiver hardware delays in code observations; ε and ξ denote the remaining errors of pseudorange and phase observations and are considered as white noise; and $\Delta\gamma_{ab}$ is the DDIFB rate. The pseudorange IFB item d_{ab}^{ij} was not considered in this study, only $\Delta\gamma_{ab}$. If IFBs are absent, Model (1) can be solved with traditional methods (Leick, 1998; Wang, 2000). Otherwise, the IFB rate $\Delta\gamma_{ab}$ needs to be estimated or corrected.

The particle filtering approach is mainly composed of three steps: the update step, the resampling step and the prediction step. In the update step, IFB rate samples with initial weights are first randomly generated and used to correct the IFB in Model (1). The corresponding RATIO values in ambiguity fixing by the Lambda method (Teunissen, 1995) are then calculated. The RATIO value was proposed in Euler and Schaffrin (1991) and indicates the closeness of the float solution to its nearest integer vector (Verhagen and Teunissen, 2013). Among the randomly generated IFB rate values, the ones that are closer to the true value can accurately calibrate the phase IFB and better recover the integer nature of the DD ambiguities, leading to a higher RATIO in the ambiguity fixing. Thus, the calculated RATIO value is used to update the weights of the IFB rate samples. Finally, the IFB rate value can be calculated as the expectation of the weighted samples. The remaining resampling step is to delete the samples with small weights, and the prediction step is to predict the sample values for the next epoch (Doucet et al., 2000; Arulampalam et al., 2002; Tian et al., 2015, 2018a).

Usually, the phase IFB for L1 and L2 has the same value for almost all baselines, therefore only one IFB rate parameter is needed for both L1 and L2 frequency data (Tian et al., 2015). However, in certain special cases, the IFB rate for L1 and L2 may differ, as presented in Wanninger (2012). To obtain the IFB rates for L1 and L2 frequencies simultaneously, the IFB estimation method was developed to a two-dimensional approach, where two unknown

https://doi.org/10.1017/S037346331900078X Published online by Cambridge University Press

IFB rate parameters for L1 and L2 are estimated simultaneously. If the x abscissa is used to represent the IFB for L1, and the y ordinate is used to represent the IFB for L2, the sample collection $\{x_i, y_i\}_{i=1}^{N}$ representing the two IFB rates can be generated in a two-dimensional area. The procedure of the two-dimensional IFB rate estimation is as follows.

Step 1: For the first epoch, generate the sample/particle collection $\{x_i, y_i\}_{i=1}^{N}$ over the initial area from [−50, −50] mm/FN to [50, 50] mm/FN for the two IFB values of L1 and L2 frequencies and assign all the particles the equal weights $w = 1/N$. For the other epoch $k = 2, 3, \ldots$, the particles have been prepared in the data processing of the last epoch $k - 1$.

Step 2: For each particle, the x and y values are set as known phase IFB rates for L1 and L2 frequencies, respectively. Calculate the float DD ambiguities and implement the ambiguity fixing via the Lambda method and calculate the RATIO values with Equation (2).

$$\text{RATIO} = \frac{\left(\hat{\boldsymbol{b}} - \check{\boldsymbol{b}}'\right)^T Q_{\hat{\boldsymbol{b}}\hat{\boldsymbol{b}}} \left(\hat{\boldsymbol{b}} - \check{\boldsymbol{b}}'\right)}{\left(\hat{\boldsymbol{b}} - \check{\boldsymbol{b}}\right)^T Q_{\hat{\boldsymbol{b}}\hat{\boldsymbol{b}}} \left(\hat{\boldsymbol{b}} - \check{\boldsymbol{b}}\right)} \tag{2}$$

where $\hat{\boldsymbol{b}}$ indicates the float solution vector of DD ambiguities; $Q_{\hat{\boldsymbol{b}}\hat{\boldsymbol{b}}}$ is the variance-covariance matrix of the float solution; $\check{\boldsymbol{b}}$ and $\check{\boldsymbol{b}}'$ are the primary and secondary candidates for the DD integer ambiguity vector for minimising $f(\boldsymbol{b}) = (\hat{\boldsymbol{b}} - \boldsymbol{b})^T Q_{\hat{\boldsymbol{b}}\hat{\boldsymbol{b}}} (\hat{\boldsymbol{b}} - \boldsymbol{b})$, respectively.

Step 3: Update the weights with the normalised RATIO. Calculate the estimated F-ISB and their particle variances by Equations (3) and (4), respectively.

$$\hat{\boldsymbol{x}}_k \approx \sum_{i=1}^{N} \boldsymbol{x}_k^i w_k^i \tag{3}$$

$$\text{var}(\hat{\boldsymbol{x}}_k) \approx \sum_{i=1}^{N} \left(\boldsymbol{x}_k^i - \hat{\boldsymbol{x}}_k\right) \left(\boldsymbol{x}_k^i - \hat{\boldsymbol{x}}_k\right)^T w_k^i \tag{4}$$

where $\boldsymbol{x}$ includes two values $[x, y]$ for the IFB rates of the L1 and L2 frequencies, respectively,

Step 4: Resample the particles if $N_{\text{eff}} = (1/\sum_{i=0}^{N} (w_k^i)^2)$ is smaller than a threshold value N_{th}, which is usually set as two thirds of the number of particles N.

Step 5: Predict the particles for the next epoch with models that simply add white noise.

Step 6: Repeat Steps 1–5 for the next epoch $k + 1$.

The above procedure is based on previous research (Tian et al., 2015, 2018a). The main difference is that the dimension of the particles increases from 1 to 2 so that the IFB rates for both the L1 and L2 frequencies can be estimated simultaneously. For example, the IFB rates for IGS baseline STR1-TIDV were estimated with both GLONASS and GPS data on DOY (day of year) 180 of 2018. At the beginning, the initial IFB rates ranged from −40 mm/FN to 40 mm/FN with a 2 mm/FN interval employed for both L1 and L2 frequencies to correct the IFB rates. The corresponding RATIO values were calculated giving results at three epochs 00:04:30, 00:13:00 and 00:49:30, which are presented in Figures 1(a)–1(c), respectively. The points with maximum RATIO values can be clearly identified and their corresponding IFB values are supposed to be the true values.

The two-dimensional RATIO value at each epoch was spread into one-dimension by plotting the rows side by side in order to present the RATIO distributions along the epoch.

https://doi.org/10.1017/S037346331900078X Published online by Cambridge University Press

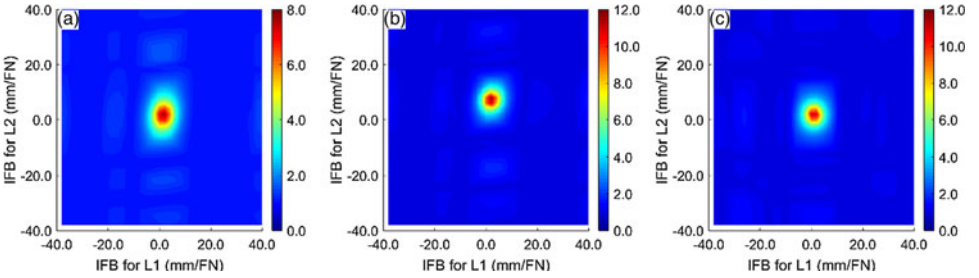

Figure 1. (a) RATIO values at epoch 00:04:30, (b) 00:13:00 and (c) 00:49:30, with GLONASS IFB rates ranging from −40 mm/FN to 40 mm/FN for both L1 and L2 frequencies.

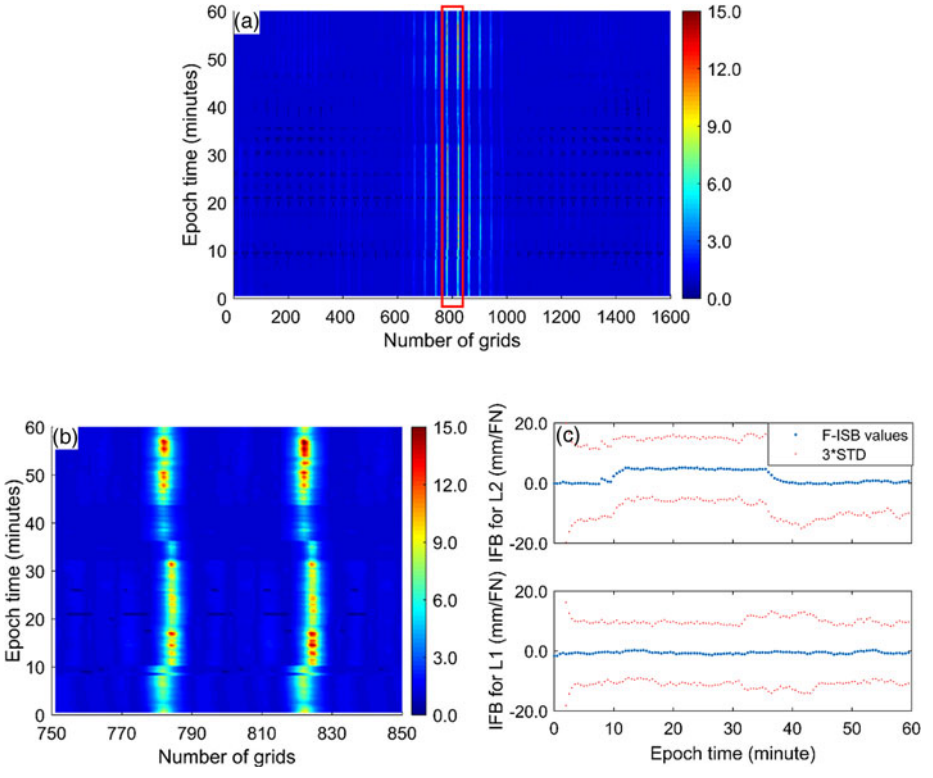

Figure 2. (a) One-dimensional RATIO distribution spread from the two-dimensional RATIO distributions, (b) the zoom-in of the area within the red box and (c) the corresponding estimated IFB rates and the three times STD of the weighted particles for L1 and L2 frequencies.

The samples ranging from −40 mm/FN to 40 mm/FN with a 2 mm/FN interval led to 40 grid values for each dimension (Figure 2) and thus a total of 1,600 grids for the one-dimensional plot. The spread of the one-dimensional RATIO values for the first 120 epochs are shown in Figure 2(a). The middle part of Figure 2(a) fromgrids 750–850 is enlarged and plotted in Figure 2(b). A change with a magnitude of several millimetres at around the 20th epoch can be observed. The estimated IFBs for both L1 and L2 by the two-dimensional

https://doi.org/10.1017/S037346331900078X Published online by Cambridge University Press

Table 1. Number of baselines for three baseline length ranges and three baseline groups.

	2011	2014	2018	Group I	Group II	Group III
0–5 km	16	41	75	102	10	20
5–10 km	3	10	13	16	6	4
10–15 km	1	4	7	7	3	2
Sum	20	55	95	125	19	26
Percent %	11·8	32·4	55·9	73·5	11·2	15·3

particle filtering approach are presented in Figure 2(c), where the change at the 20th epoch is clearly visible. The two-dimensional method is capable of estimating the IFB rates of the L1 and L2 frequencies simultaneously and is employed in the following calculations.

3. DATA OF SHORT BASELINES FOR IFB RATE ESTIMATION. All data collected on DOY 365 of 2011, DOY 365 of 2014 and DOY 108 of 2018 of the GLONASS baselines shorter than 15 km in the EUREF and IGS GNSS networks were downloaded and analysed. The data for one day were sampled at a time interval of 30 s and included a total of 170 baselines. The number of baselines with a length of 0–5 km, 5–10 km and 10–15 km are shown in Table 1. Some of the baselines for the 3 days had the same name but usually with different receivers or series. If the distances among three receivers were shorter than 15 km, only two independent baselines were counted. Thus, all 170 baselines were considered independent.

In the calculations, not all GLONASS baselines could be successfully solved, that is, have validated fixed solutions with a RATIO threshold value of 3 when the IFB rates were known. The failed baselines had lengths falling within all three ranges 0–5 km, 5–10 km and 10–15 km. Unmodeled error sources, such as multipath effects, high spatial variation of the troposphere, and equipment malfunctions, could have been responsible for the failure. Failed baselines cannot provide accurate IFB rate estimates and should be excluded. Therefore, the baselines were further classified into three groups according to the characters of the RATIO values corresponding to the two-dimensional IFB rate area from [−40, −40] mm/FN to [40, 40] mm/FN. The first group had validated fixed solutions with large RATIO values corresponding to the true IFB rates and was designated Group I. Group II also had fixed solutions but with a much lower RATIO. The third group (III) had almost no fixed solutions even with correct IFB rates. The examples of the ratio distributions for the three groups are shown in Figure 3, where Figure 3(a) presents baseline HERS_HERT belonging to Group I, Figure 3(b) presents baseline HEL2_HELG belonging to Group II, and Figure 3(c) presents LCK3_LCK4 belonging to Group III.

For Group I, IFB rates could be estimated rapidly and accurately. With accurate IFB rate values, the integer ambiguities of baselines can be resolved with a much larger RATIO. The IFB rates of Group II could also be estimated, but the ambiguity fixing had a much smaller RATIO. The sample variance calculated by Equation (4) was large and the convergence time was longer. The IFB rates for Group III could not be estimated, that is, the fixed solutions of the baselines could not be solved even with accurate IFB rate values. The number of baselines for each group were counted and given in Table 1. The percentages of the baselines for the three groups were 73·7%, 11·1% and 15·2%, respectively.

The proportions for Group I were 77·3%, 61·5% and 58·3% for the three ranges 0–5 km, 5–10 km and 10–15 km, respectively. The percentage decreases as the baseline

https://doi.org/10.1017/S037346331900078X Published online by Cambridge University Press

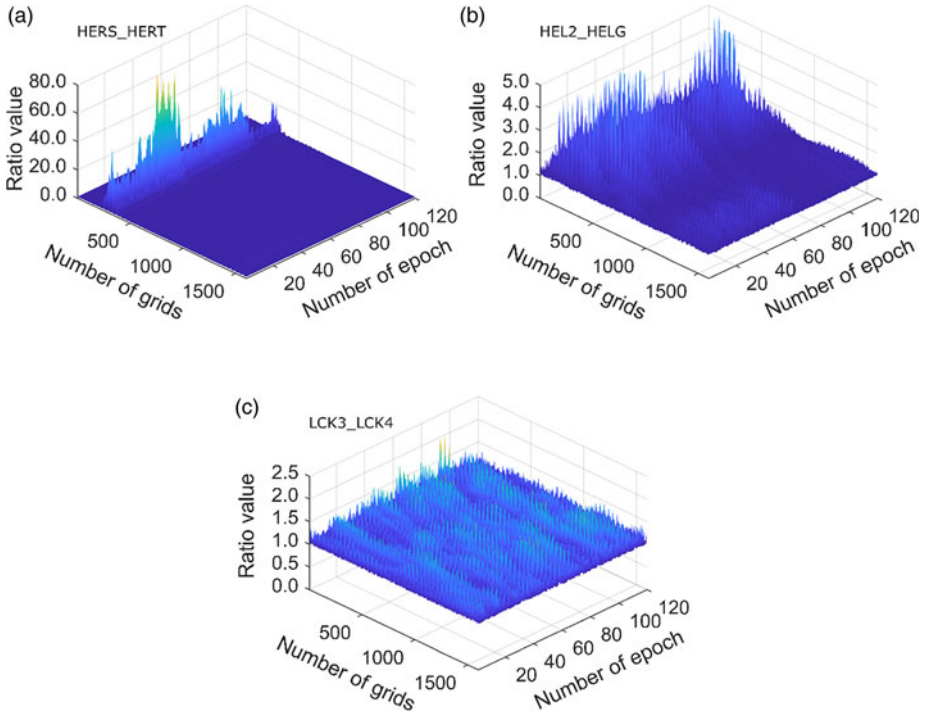

Figure 3. One-dimensional RATIO distributions spread from two-dimensional distributions for the first 120 epochs. (a) The figures are for baseline HERS_HERT belonging to Group I, (b) baseline HEL2_HELG belonging to Group II and (c) baseline LCK3_LCK4 belonging to Group III.

Table 2. Number of baselines for different receiver combinations.

	TRI	JAV	JPS	LEI	SEP	TPS
TRI	6					
JAV	16	4				
JPS		7	2			
LEI	14	3	1	11		
SEP	6	5		8	2	
TPS	5	10	2	7	2	13
ASH	1					

length increases; this is probably due to an increase in the length-related errors in the models, such as atmosphere delays and multipath effects. Those errors are supposed to be very small for ultra-short baselines and become larger as the baseline length increases.

The Group I baseline included receivers from seven manufacturers including Javad (JAV), JPS, Leica (LEI), Septentrio (SEP), TPS, Trimble (TRI) and Ashtech (ASH), which occupied 96·9% of all 489 IGS stations with data available on DOY 180 of 2018. The number of baselines for each Group I receiver combination were counted and are presented in Table 2. The number of baselines with receivers from different manufactures was 87, and from the same manufacturer was 38.

https://doi.org/10.1017/S037346331900078X Published online by Cambridge University Press

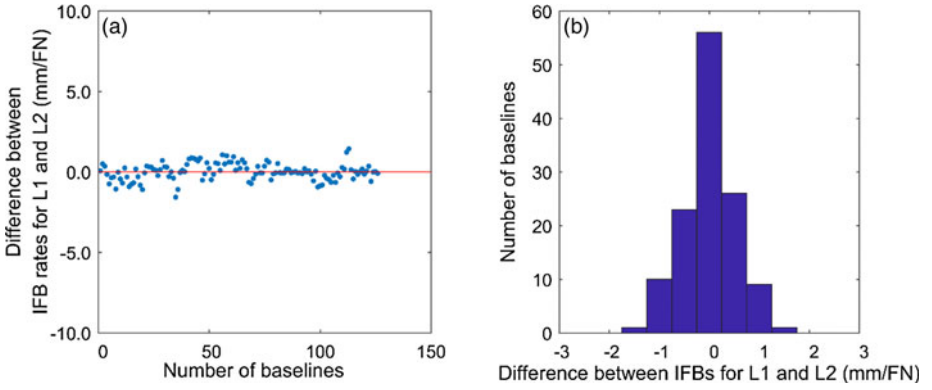

Figure 4. (a) Differences between IFB rates of L1 and L2 for the 125 baselines of Group I, and (b) the corresponding histogram of those differences.

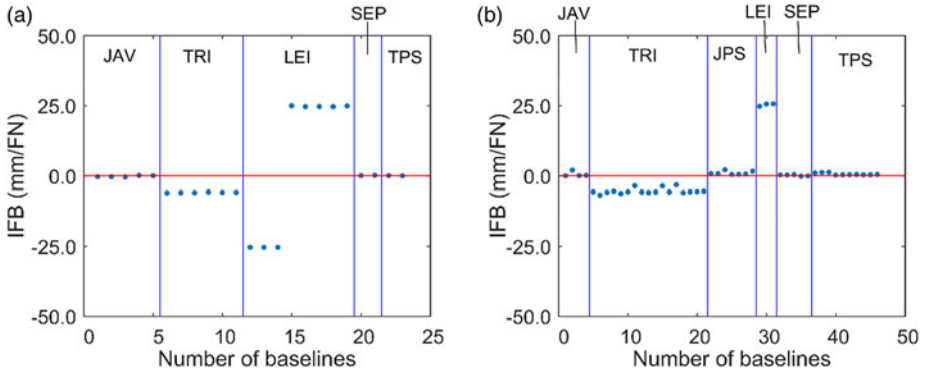

Figure 5. (a) IFB rates of the baselines for Septentrio receivers and (b) the values for Javad receivers.

4. ANALYSIS AND REFINEMENT OF IFB RATE ESTIMATES. Among the three groups outlined in Section 3, only Group I was selected to estimate the IFB rates because those baselines could provide the most accurate estimates. After the IFB rate values for L1 and L2 were estimated, their differences were calculated. The values of the differences had a standard deviation (SD) of 0·53 mm/FN, which are plotted in Figure 4(a) with a corresponding histogram shown in Figure 4(b). Almost all 125 baselines had an IFB rate for L1 equal to that of L2. Rare exceptions, with millimetre-level differences within a short time frame, were found, such as the results shown in Figure 2(c), again, probably due to unmodeled system errors.

In the following investigation, the IFB rates for L1 and L2 were considered to be the same and their mean value was analysed. For example, the mean IFB rates for Septentrio and JPS, Javad and JPS receivers are plotted in Figures 5(a)–5(b), respectively. The IFB rate values for the same receiver combinations were very similar. Although Javad receivers are more divergent, as highlighted in previous studies (Wanninger 2012), they show better consistency (Figure 5(b)).

https://doi.org/10.1017/S037346331900078X Published online by Cambridge University Press

Table 3. Value Set 1 of IFB rates and its difference with Value Set 2 and Value Set 3.

Receiver manufacturers	IFB (mm/FN)	SD (mm/FN)	Difference between Value Sets 1 and 2	Difference between Value Sets 1 and 3
TRI	−6·5	0·2	0·5	−1·2
JAV	−1·0	0·2	−1·0	−0·3
JPS	0·0	0·0	0·0	0·0
LEI	23·9	0·2	0·9	0·4
SEP	−0·7	0·3	–	−1·0
SEP2	49·2	0·5	0·2	0·1
TPS	−0·2	0·2	−0·2	–
ASH	4·2	0·7	0·2	1·3

Afterwards, the IFB rates of the 87 baselines with receivers from different manufacturers were adjusted by the least-squares method to derive statistically more accurate values. For a total of seven receiver brands, eight unknown IFB rate parameters needed refining. The number of unknown parameters was larger by one because the Septentrio receivers have two different IFB rates for the series before POLARX3ETR and after POLARX4ETR (Jiang et al., 2017). The IFB rate of the JPS receivers were set as the reference receiver with an IFB rate of zero to be consistent with the previous studies. Changing the reference receiver may lead to different adjustment results but will not affect the relative IFB rate values that really matter in relative positioning. In the least-squares calculations, 87 observation equations were formed with uniform weights. An additional constraint equation with much larger weights was added to assign zero as the IFB rate of the JPS receivers. The equation set (Equation (5)) follows.

$$v = Ax - L \tag{5}$$

where

$$A = \begin{bmatrix} -1, 1, 0, 0, 0, 0, 0, 0 \\ -1, 0, 1, 0, 0, 0, 0, 0 \\ \vdots \\ 0, 0, 0, 0, 0, 0, -1, 1 \\ 0, 0, 0, 0, 0, 0, 0, 1 \end{bmatrix}, x = \begin{bmatrix} \\ \mathrm{IFB}_{01} \\ \mathrm{IFB}_{02} \\ \vdots \\ \mathrm{IFB}_{08} \end{bmatrix} \text{ and } L = \begin{bmatrix} \mathrm{IFB}_{12} \\ \mathrm{IFB}_{13} \\ \vdots \\ \mathrm{IFB}_{88} \\ \mathrm{IFB}_{08} \end{bmatrix}.$$

v is the residual vector, A is the coefficient matrix, x is the unknown vector with elements $[\mathrm{IFB}_{01}, \mathrm{IFB}_{01}, \ldots, \mathrm{IFB}_{08}]$ representing the unknown IFB rates, and L is the relative IFB rate vector estimated by particle filtering. The last line of Matrix A has a different form from other lines because this line is the equation that assigns the IFB rate parameter of the reference receiver type as zero, whereas other lines are relative IFB rate equations, so is the last element of vector L.

The refined IFB rate values and the corresponding SD are shown in Table 3. The variance of unit weight is represented by $\sigma_0^2 = v^T P v / n - t = 0 \cdot 44$ mm/FN. With those solutions, the residuals of the equation sets are plotted in Figure 6(a), and the histogram of the residuals is shown in Figure 6(b).

For convenience of comparison, the refined IFB rate values are denoted as Value Set 1. The IFB values given by Wanninger (2012) are referred to as Value Set 2, and the values given by Jiang (2017) are denoted as Value Set 3. The differences between the

https://doi.org/10.1017/S037346331900078X Published online by Cambridge University Press

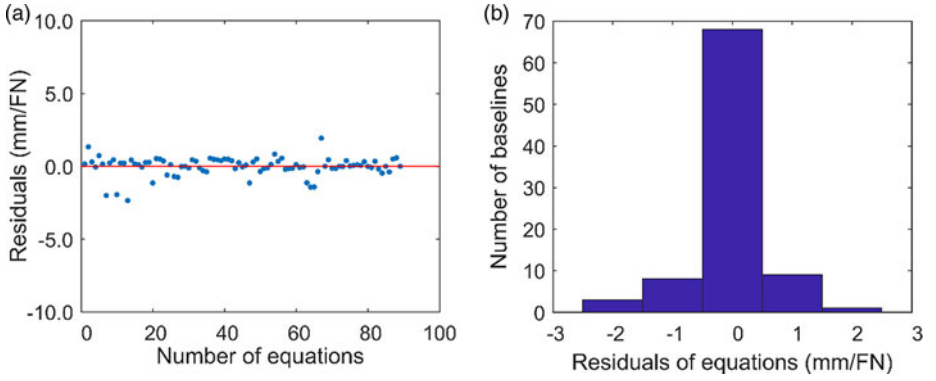

Figure 6. (a) Residuals of the 87 baselines with different receiver brands and (b) the histogram of those residuals.

three value sets are presented in Table 3. The magnitude of the maximum difference in Table 3 for Value Set 1 and Value Set 2 is 1·0 mm/FN, and for Value Set 1 and Value Set 3 is 1·3 mm/FN. JPS was the reference receiver for all three value sets (Table 3). When combinations of all receiver brands were considered, the maximum difference increased. For example, the difference for a TRI_ASH combination between Value Set 1 and Value Set 3 was 2·5 mm/FN. In the following sections, the effects of the IFB rate differences on the empirical success rate of single-epoch ambiguity fixing for GLONASS-only and for GPS/GLONASS integration will be investigated.

5. INVESTIGATION OF THE SINGLE-EPOCH AMBIGUITY FIXING WITH REFINED IFB RATES. Ambiguity fixing in GNSS single-epoch positioning is crucial for precision. If the integer ambiguities are reliably fixed, sub-centimetre-level horizonal positions can be achieved for short baselines; if not, positioning accuracy will be low and the results equal to those calculated with pseudorange measurements. Therefore, IFB calibration affecting ambiguity fixing is important for positioning accuracy. For example, GLONASS data collected on DOY 180 of 2018 with a 30-s epoch interval were employed to solve the baseline MATG_MATZ with a length of 21·5 m. The pseudorange IFBs of the baseline were calibrated in advance using the look-up table method (Tian et al., 2018b) and the RATIO test with threshold of 3 was employed in the ambiguity fixing. The horizontal solutions with and without phase IFB calibration of IFB rate −24·6 mm/FN are plotted in Figure 7. The fixed solutions with IFB calibration represented by blue dots are much more accurate than the grey and red dots denoting the solutions without IFB calibrations.

The empirical success rate of ambiguity fixing decreases quickly due to the increment of the IFB rate error, as shown in Figure 8(a). Furthermore, the success rate of ambiguity fixing is highly correlated with positioning accuracy, such as in the plot of the baseline length SD against the empirical success rate, shown in Figure 8(b).

In the following sections, the empirical success rates of ambiguity fixing for both the GLONASS-only and the GPS/GLONASS combination single-epoch positioning are calculated and analysed. In the GLONASS-only applications, different baselines are resolved with the same satellite cut-off elevation angle of 12°, while in the GPS/GLONASS combination different satellite cut-off elevation angles are used.

https://doi.org/10.1017/S037346331900078X Published online by Cambridge University Press

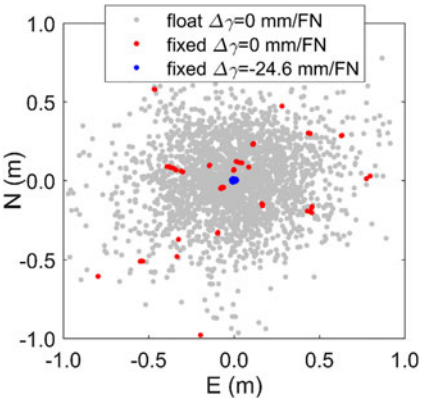

Figure 7. GLONASS horizontal solutions for baseline MATG_MATZ with data collected on DOY 180 of 2018 with and without IFB calibrations. The grey dots and the red dots represent the float and fixed solutions without IFB calibration, respectively, and the blue dots are the fixed solutions with IFB calibration.

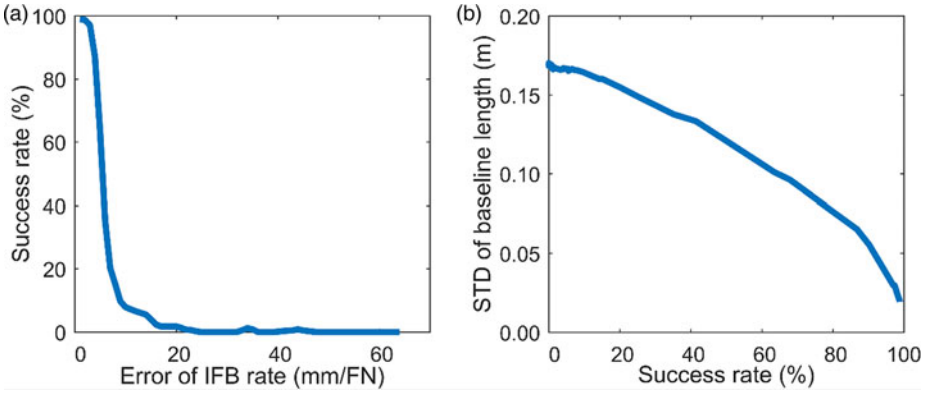

Figure 8. (a) Empirical success rates for different IFB rate errors and (b) the SD of the estimated baseline length for different empirical success rates for baseline MATG_MATZ with data collected on DOY 180 of 2018.

5.1. *Empirical success rates of ambiguity fixing for GLONASS-only positioning.* The relatively large differences between the refined IFB rate value and the values given in previous studies including combinations of SEP_LEI, TRI_LEI, JAV_LEI and TRI_ASH are listed in Table 4. The empirical success rates of ambiguity fixing with those IFB rates were investigated with the short baselines.

Firstly, six short baselines were employed for SEP_LEI. As shown in Table 4, the IFB rate for the SEP_LEI combination is −24·6 mm/FN for Value Set 1, which differs from Value Set 3 by 1·4 mm/FN. Value Set 2 did not provide a SEP IFB rate, therefore there was no data. The empirical success rates of ambiguity fixing with IFB rates ranging from −50 mm/FN to 0 mm/FN are presented in Figure 9(a). The values of the empirical success rates change according to different IFB rates. The IFB rate for Value Sets 1 and 3 are highlighted in Figure 9(a) with blue and red lines, respectively, and the corresponding

https://doi.org/10.1017/S037346331900078X Published online by Cambridge University Press

Table 4. IFB rates and average success rates of Value Set 1 and the differences in relation to Value Set 2 (1–2) and Value Set 3 (1–3) for the four receiver combinations in Figure 9.

Receiver combinations	IFB rate (mm/FN)			No. of baselines	Average success rate (%)		
	1	1–2	1–3		1	1–2	1–3
SEP_LEI	−24·6	–	−1·4	6	57·8	–	20·6
TRI_LEI	−30·4	−0·4	−1·6	16	40·7	2·6	18·5
JAV_LEI	−24·9	−1·9	−0·7	6	85·0	24·2	4·6
TRI_ASH	−10·7	0·3	−2·5	1	66·8	−0·1	11·8

empirical success rates of the two value sets are shown in Figure 9(b). With the IFB rate from Value Set 1, the success rates for all six baselines improved by an average of 20·6%.

The TRI_LEI combination baselines were then resolved. The IFB rate was −30·4 mm/FN for Value Set 1, and −30 mm/FN and −28·8 mm/FN for Value Sets 2 and 3, respectively. Sixteen data sets in total were employed and their empirical success rates of ambiguity fixing with different IFB rates were calculated and plotted in Figure 9(c). The IFB rate for Value Sets 1, 2 and 3 are also indicated in Figure 9(c) with blue, green and red lines, respectively. The success rates for the three value sets are shown in Figure 9(d). The main success rate difference was between Value Set 1 and Value Set 3, where an average improvement of 18·5% was observed.

For the JAV_LEI combination, the main difference, −1·9 mm/FN, was between Value Sets 1 and 2. Six baselines were employed. The success rates corresponding to the IFB rates from −50 mm/FN to 0 mm/FN are shown in Figure 9(e), while the success rates for the IFB rates for the three value sets are presented in Figure 9(f). The IFB rate of Value Set 1 showed superior performance with an average success rate 24·2% higher than Value Set 2. However, the WTZR_WTZZ baseline was different from the others as Value Set 2 achieved a higher success rate than Value Set 1. This indicates that not all the baselines have exactly the same IFB rate. However, although certain cases showing slight variation exist, Value Set 1 was generally preferable.

For the TRI_ASH combination, only one short baseline, CTDA_RVDI, was available. Its success rate corresponding to IFB rates from −50 mm/FN to 0 mm/FN is plotted in Figure 9(g). The magnitude of Value Set 1 is very close to Value Set 2 but is 2·5 mm/FN away from Value Set 3, leading to an improvement of 11·8% on the success rate of ambiguity fixing compared with Value Set 3. The peaks of the ambiguity fixing success rates in Figures 9(a), 9(c) and 9(e) cluster around a certain IFB rate value. The IFB rates of Value Set 1 are around those peaks, and expectations for the empirical success rate of the ambiguity fixing are larger. As a result, the IFB rates of Value Set 1 were able to provide significantly better performance on ambiguity fixing than Value Sets 2 and 3.

5.2. *Empirical success rates of ambiguity fixing for GPS/GLONASS combination positioning.* The GPS/GLONASS combination positioning has more available satellites and thus is superior to positioning with a single satellite constellation. The success rates of ambiguity fixing with cut-off elevation angles from 10–50° with an interval of 10° were investigated.

Six short baselines with receiver combinations JAV_LEI, TRI_LEI, SEP_LEI and TRI_ASH, as listed in Table 4, were taken as examples. The lengths of the baselines

https://doi.org/10.1017/S037346331900078X Published online by Cambridge University Press

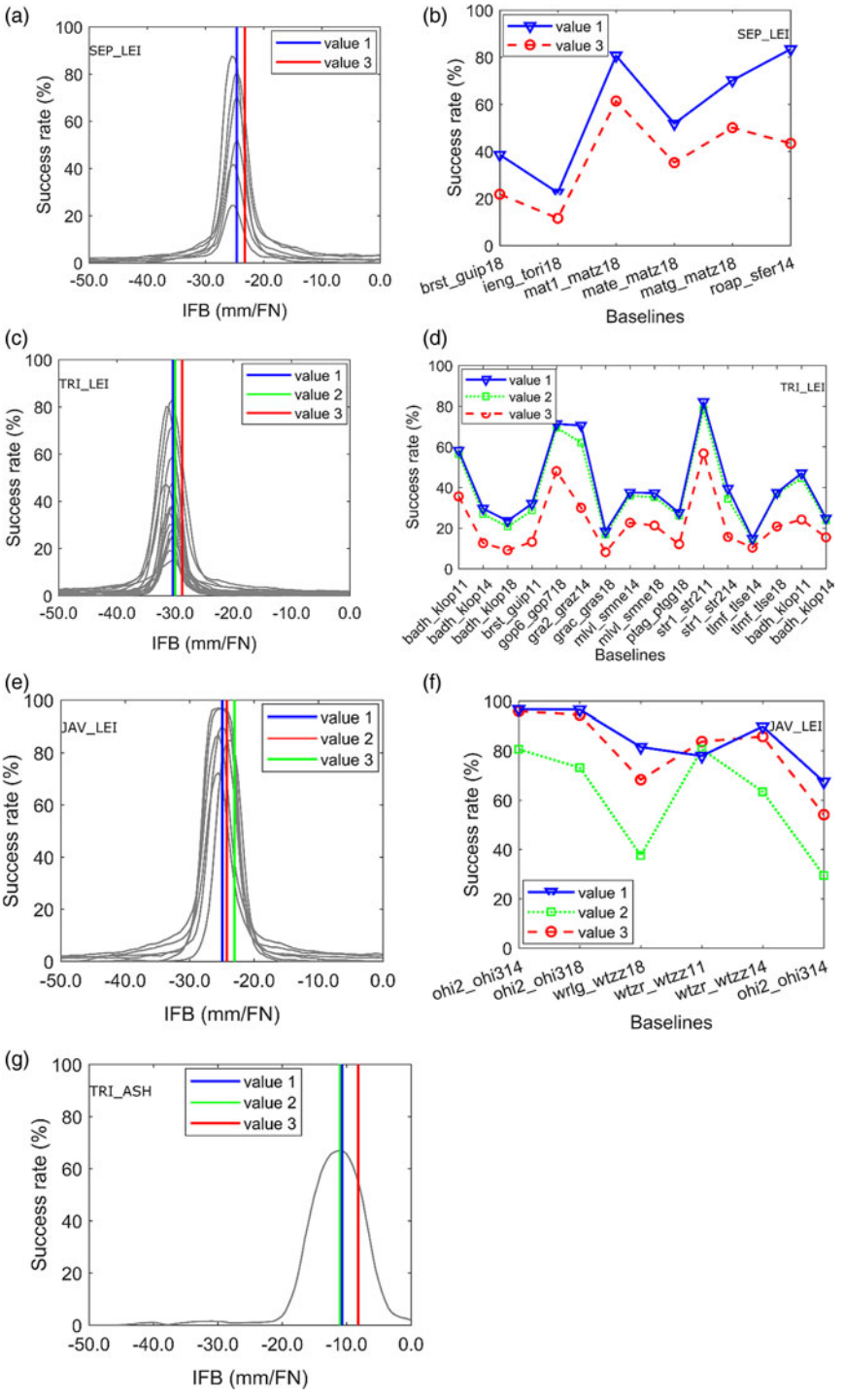

Figure 9. Empirical success rates of the ambiguity fixing for the baselines of (a) SEP_LEI, (c) TRI_LEI, (e) JAV_LEI and (g) TRI_ASH with IFB rates from −50 mm/FN to 0 mm/FN, and the empirical success rates corresponding to the three value sets for (b) SEP_LEI, (d) TRI_LEI and(f) JAV_LEI.

https://doi.org/10.1017/S037346331900078X Published online by Cambridge University Press

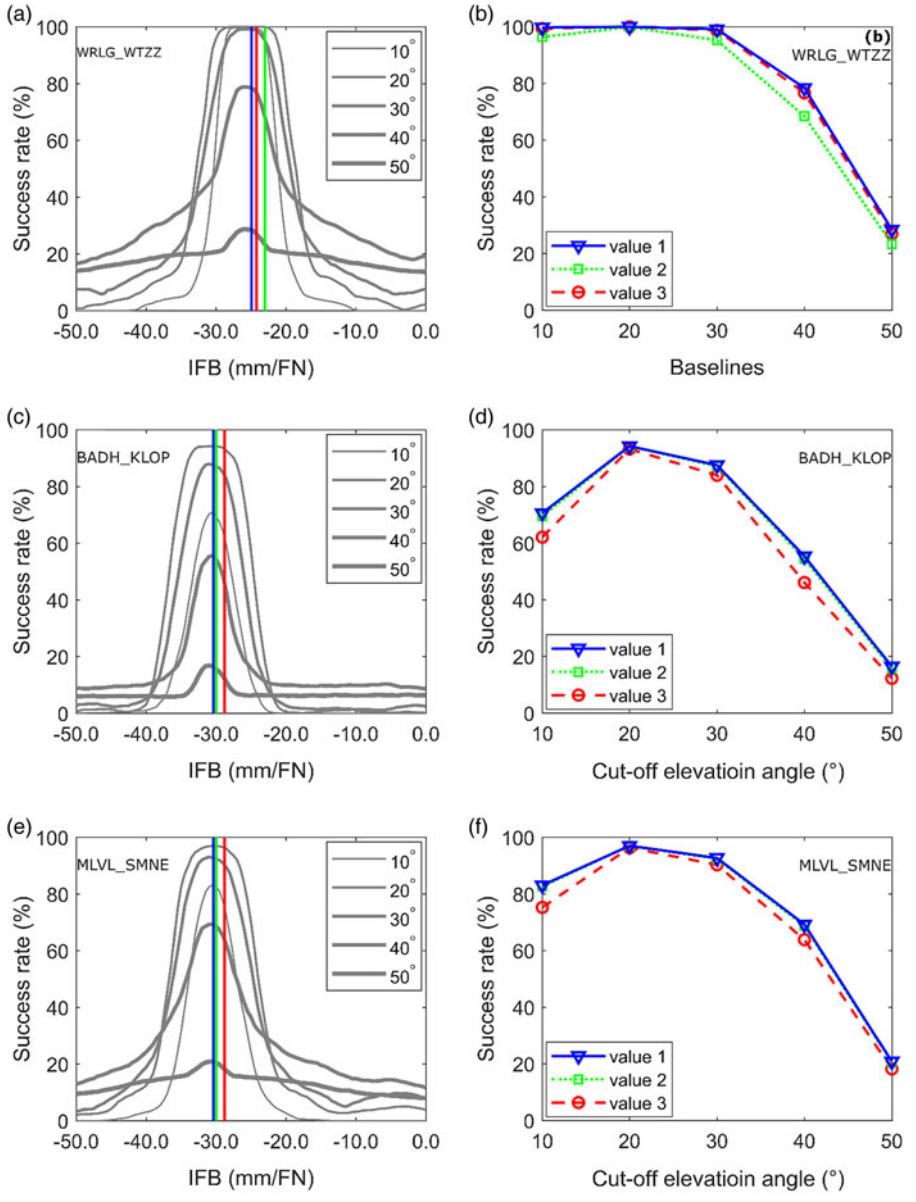

Figure 10. Empirical success rates of the ambiguity fixing with different cut-off elevation angles for IFB rates ranging from −50 mm/FN to 0 mm/FN (a, c, e, g, i, k), and for the IFB rates of the three value sets (b, d, f, h, j, l).

ranged from 258·3 m to 11,918·6 m. The success rates of ambiguity fixing corresponding to different IFB rates from −50 mm/FN to 0 mm/FN for the six baselines are plotted in Figures 10(a), 10(a), 10(c), 10(e), 10(g), 10(i) and 10(k) respectively. When the cut-off elevation angle was set to 10°, the peaks of the plot were relatively narrow. The narrow peaks indicate that the empirical success rates are very sensitive to IFB rates. The peaks become wider for a cut-off angle of 20°, indicating the empirical success rates are

https://doi.org/10.1017/S037346331900078X Published online by Cambridge University Press

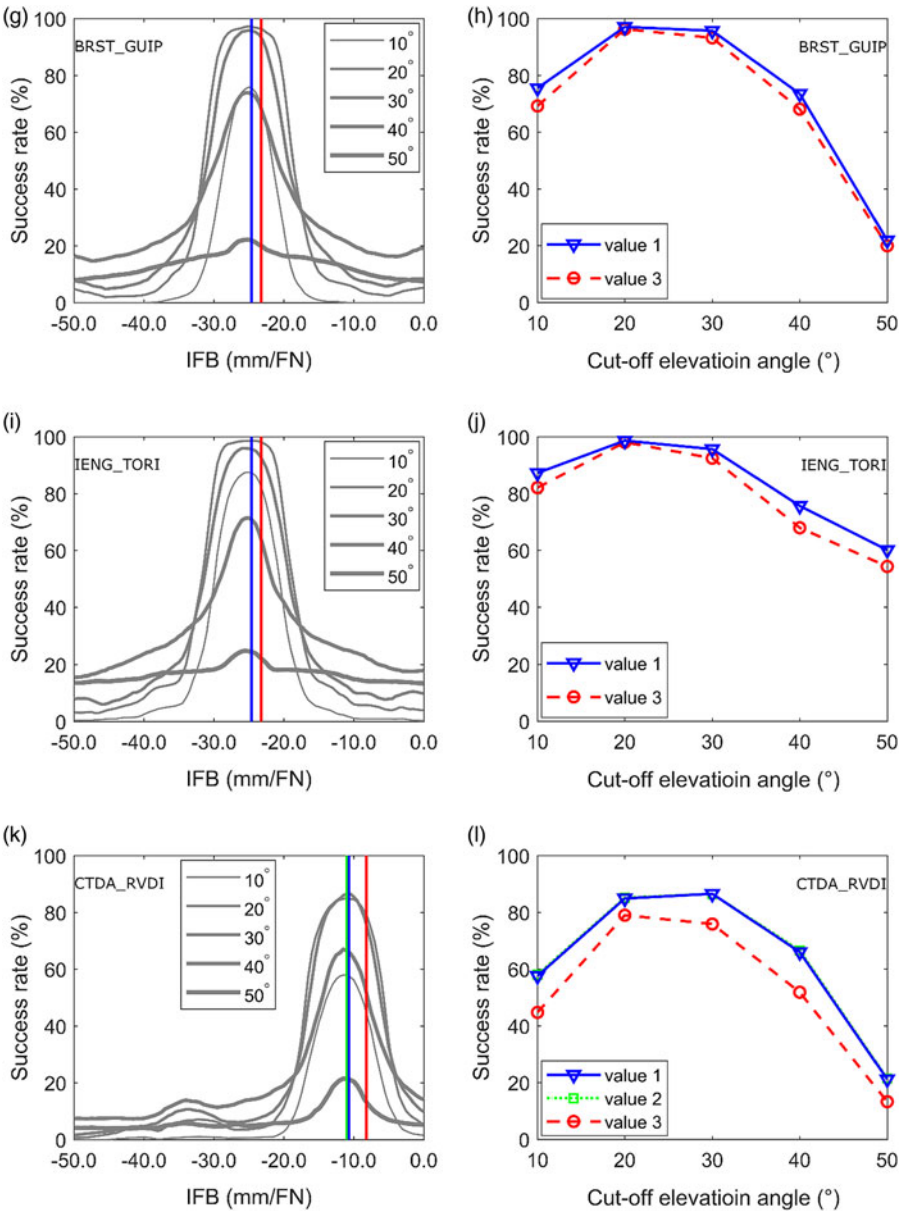

Figure 10. Continued.

less sensitive to IFB rates. All three of the IFB rates from the three value sets for each receiver combination achieved similar results. As the cut-off elevation angle increased to 30° or larger, the shape of the line became narrow again. This probably because the models have larger observation errors with a cut-off elevation angle of 10° and fewer observed satellites for 30°, thus even a small IFB rate error could lead to a noticeable decrease in the empirical success rate. The models with a cut-off elevation angle of 20°

https://doi.org/10.1017/S037346331900078X Published online by Cambridge University Press

Table 5. Baselines employed for GPS/GLONASS combination experiments and the achieved maximum improvements with IFB Value Set 1 compared with Value Set 2 (1–2) and Value Set 3 (1–3).

Baselines	Receiver combinations	Length (m)	Maximum improvement (%)/ cut-off elevation angle/value set
WRLG_WTZZ	JAV_LEI	258·3	10·0/40°/1–2
BADH_KLOP	TRI_LEI	8627·4	9·3/40°/1–3
MLVL_SMNE	TRI_LEI	11,918·6	7·8/10°/1–3
BRST_GUIP	SEP_LEI	9498·3	6·3/10°/1–3
IENG_TORI	SEP_LEI	5630·7	7·2/40°/1–3
CTDA_RVDI	TRI_ASH	6762·8	14·2/40°/1–3

were not seriously affected by the two factors and could tolerate relatively large IFB rate errors.

The empirical success rates of the ambiguity fixing corresponding to the three IFB value sets are presented in Figures 10(b), 10(d), 10(f), 10(h), 10(j), and 10(l). For the six baselines, the largest improvement was seen at a cut-off elevation angle of 10° or 40°. The maximum improvement on empirical success rates for Value Set 1 ranged from 6·3% to 14·2% for the six baselines, as shown in Table 5.

6. CONCLUSIONS. The ambiguity fixing in GLONASS precise positioning requires accurate phase IFB calibration. This study refined the IFB rates based on short baselines of IGS and EUREF via a two-dimensional particle filtering approach, and then investigated the applications of those IFB rates on GLONASS single-epoch ambiguity fixing.

The refined IFB rates differed to the values given in previous studies for some receiver combinations, for example, 1·4 mm/FN for Septentrio and Leica receivers, 1·6 mm/FN for the Trimble and Leica receivers, and 2·5 mm/FN for the Trimble and Ashtech receivers. GLONASS ambiguity fixing in single-epoch data processing was found to be very sensitive to the IFB rate error. The empirical success rates of ambiguity fixing were significantly improved with the refined IFB rate values. For example, the 1·4 mm/FN difference between Septentrio and Leica receivers improved the empirical success rate by an average of 20·6% with six baseline data sets, and the 1·6 mm/FN difference between Trimble and Leica receivers led to an average improvement of 18·5% with 16 baseline data sets. For GPS/GLONASS integration, IFB rates can also obviously affect the empirical success rates of the ambiguity fixing and their effects vary according to different cut-off elevation angles. The millimetre errors in the IFB rate may not degrade the success rate significantly at a cut-off elevation angle of 20°, but at 10° and 40° the effects can be large, as in the 14·2% for baseline CTDA_RVDI with Trimble and Ashtech receivers. The refined IFB rate values achieved significantly higher empirical success rates for single-epoch ambiguity fixing. It is our hope that this research will prove very helpful to the study and application of rapid GLONASS and multi-GNSS positioning.

ACKNOWLEDGEMENTS

This work was supported by the Young Scientists Fund of the National Natural Science Foundation of China (Grant No. 41804022), the Fundamental Research Funds for the Central Universities (Grant

No. 2682018CX33) and the State Key Laboratory of Geodesy and Earth's Dynamics (Institute of Geodesy and Geophysics, CAS) (Grant No. SKLGED2018-3-1-E).

REFERENCES

Al-Shaery, A., Zhang, S. and Rizos, C. (2013). An enhanced calibration method of GLONASS inter-channel bias for GNSS RTK. *GPS Solut*ions, **17**(2), 165–173.

Arulampalam, M. S., Maskell, S., Gordon, N. and Clapp, T. (2002). A tutorial on particle filters for online nonlinear/non-Gaussian Bayesian tracking. *IEEE Transactions on Signal Processing*, **50**(2), 174–188.

Banville, S., Collins, P. and Lahaye, F. (2013). GLONASS ambiguity resolution of mixed receiver types without external calibration. *GPS Solutions*, **17**(3), 275–282.

Doucet, A., Godsill, S. and Andrieu, C. (2000). On sequential Monte Carlo sampling methods for Bayesian filtering. *Statistics and Computing*, **10**(3), 197–208.

Euler, H. and Schaffrin, B. (1991). On a Measure of Discernibility Between Different Ambiguity Solutions in the Static-Kinematic GPS-Mode. *Proceedings of the International Symposium on Kinematic Systems in Geodesy, Surveying, and Remote Sensing*, 285–295. Springer, New York.

Jiang, W., An, X., Chen, H. and Zhao, W. (2017). A new method for GLONASS inter-frequency bias estimation based on long baselines. *GPS Solutions*, **21**(4), 1765–1779.

Leick, A. (1998). GLONASS satellite surveying. *Journal of Surveying Engineering*, **124**(2), 91–99.

Liu, Y., Ge, M., Shi, C., Lou, Y., Wickert, J. and Schuh, H. (2016). Improving integer ambiguity resolution for GLONASS precise orbit determination. *Journal of Geodesy*, **90**(8), 715–726.

Parkins, A. (2011). Increasing GNSS RTK availability with a new single-epoch batch partial ambiguity resolution algorithm. *GPS Solutions*, **15**, 391–402.

Paziewski, J. and Wielgosz, P. (2014). Assessment of GPS + Galileo and multi-frequency Galileo single-epoch precise positioning with network corrections. *GPS Solutions*, **18**, 571–579.

Pratt, M., Burke, B. and Misra, P. (1998). Single-Epoch Integer Ambiguity Resolution With GPS-GLONASS L1-L2 Data. *Proceedings of ION GPS, Institute of Navigation*, Nashville, TN, September, 389–398.

Sleewagen, J., Simsky, A., Wilde, W. D., Boon, F. and Willems, T. (2012). Demystifying GLONASS inter-frequency carrier phase biases. *Inside GNSS*, **7**(3), 57–61.

Teunissen, P. J. (1995). The least-squares ambiguity decorrelation adjustment: a method for fast GPS integer ambiguity estimation. *Journal of Geodesy*, **70**(1–2), 65–82.

Tian, Y., Ge, M. and Neitzel, F. (2015). Particle filter-based estimation of inter-frequency phase bias for real-time GLONASS integer ambiguity resolution. *Journal of Geodesy*, **89**(11), 1145–1158.

Tian, Y., Ge, M., Neitzel, F., Yuan, L., Huang, D., Zhou, L. and Yan, H. (2018a). Improvements on the particle-filter-based GLONASS phase inter-frequency bias estimation approach, *GPS Solutions*, **22**(3). doi:10.1007/s10291-018-0735-9

Tian, Y., Liu, Z., Ge, M. and Neitzel, F. (2018b). Determining inter-system bias of GNSS signals with narrowly spaced frequencies for GNSS positioning. *Journal of Geodesy*, **92**(8), 873–887.

Verhagen, S. and Teunissen, P. (2013). The ratio test for future GNSS ambiguity resolution. *GPS Solutiions*, **17**, 535–548.

Wang, J. (2000). An approach to GLONASS ambiguity resolution. *Journal of Geodesy*, **74**(5), 421–430.

Wanninger, L. (2012). Carrier-phase inter-frequency biases of GLONASS receivers. *Journal of Geodesy*, **86**(2), 139–148.

Zinoviev, A. E., Veitsel, A. V. and Dolgin, D. A. (2009). Renovated GLONASS: Improved Performances of GNSS Receivers. *Proceedings of ION GNSS 2009*, 3271–3277.